The Astrophysical Journal, 635:1151–1165, 2005 December 20

DARK CLOUD CORES AND GRAVITATIONAL DECOUPLING FROM TURBULENT FLOWS

Eric Keto[1] and George Field[1]

Received 2005 February 25; accepted 2005 August 25

ABSTRACT

We test the hypothesis that the starless cores may be gravitationally bound clouds supported largely by thermal pressure by comparing observed molecular line spectra to theoretical spectra produced by a simulation that includes hydrodynamics, radiative cooling, variable molecular abundance, and radiative transfer in a simple one-dimensional model. The results suggest that the starless cores can be divided into two categories: stable starless cores that are in approximate equilibrium and will not evolve to form protostars, and unstable prestellar cores that are proceeding toward gravitational collapse and the formation of protostars. The starless cores might be formed from the interstellar medium as objects at the lower end of the inertial cascade of interstellar turbulence. In addition, we identify a thermal instability in the starless cores. Under particular conditions of density and mass, a core may be unstable to expansion if the density is just above the critical density for the collisional coupling of the gas and dust so that as the core expands, the gas-dust coupling that cools the gas is reduced and the gas warms, further driving the expansion.

Subject headings: ISM: individual (L1544, B68, L1517B) — ISM: molecules — radiative transfer — stars: formation

Online material: color figures

1. INTRODUCTION

Observations of molecular clouds show a power-law dependence between the size (length and mass) scales of the clouds and the velocity dispersion within the clouds that extends from the largest giant molecular clouds down to the scale at which the turbulent velocities become subsonic (Larson 1981; Leung et al. 1982; Myers 1983; Sanders et al. 1985; Dame et al. 1986; Fuller & Myers 1992). The spectrum matches that expected in a turbulent cascade, suggesting that the clouds are hierarchical structures in a supersonic turbulent flow (Mac Low & Klessen 2004; Elmegreen & Scalo 2004; Scalo & Elmegreen 2004). The power-law relationships between the mass, length, and velocity dispersion also fit the relation of virial equilibrium, $\sigma_v^2 \sim 2GM/L$, as if the clouds were gravitationally bound structures. In a picture of the interstellar medium dominated by turbulence, the relationship of apparent virial equilibrium reflects a dynamic equipartition as a result of the coupling between kinetic and potential energies in the turbulent flow rather than a static equilibrium within gravitationally bound clouds (Larson 1981; Ballesteros-Paredes et al. 1999; Klessen et al. 2005). While gravity may be largely responsible for generating the supersonic flows that form the clouds, the clouds themselves are the result of compression due to inertial forces in the turbulent hydrodynamics. Clouds are formed where converging streams in the turbulence create zones of high-density gas, but these clouds formed by compression may just as easily dissipate as the flows change direction and velocity on a crossing timescale. In the inertial range of the interstellar turbulence, there are no clouds with an internal equilibrium between self-gravity and the supporting forces of thermal, turbulent, or magnetic pressure. Gravitationally bound clouds may form if the compression is strong enough to boost the local gas density beyond gravitational instability. However, these clouds will be short-lived, collapsing to form stars within a free-fall time. In the theory of the turbulent interstellar medium, these are the only gravitationally bound clouds, and star formation takes place within these collapsing clouds within one crossing time (Elmegreen 2000). The inefficiency or slow rate of star formation is then attributed to the inefficiency in the formation of these gravitationally bound clouds in the turbulent interstellar medium.

While the theory of the turbulent interstellar medium does not predict any molecular clouds in equilibrium, the observed properties of the small molecular clouds at the low end of the cloud mass spectrum known as starless cores are remarkably well described as discrete dynamical units of stable, bound gas with an internal balance of forces. These starless cores are dense regions ($n_{\rm H_2} \sim 10^4$–10^6 cm^{-3}) in dark clouds with linear scales of tenths of pc and total masses of a few solar masses. The starless cores contain no infrared sources above the sensitivity level of the *Infrared Astronomical Satellite* (*IRAS*; about 0.1 $L_\odot$ at the distance of Taurus) and thus are thought to be sites of possible future rather than current star formation (Myers et al. 1983; Myers & Benson 1983; Benson & Myers 1989; Beichman et al. 1986; Ward-Thompson et al. 1994; Tafalla et al. 1998; Lee & Myers 1999; Lee et al. 2001).

Observations of dust column density in the starless cores appear approximately as expected for cores in hydrostatic equilibrium. The observed density profiles are characterized by a core-envelope structure with an inner region of weakly decreasing density and a surrounding envelope with a steeper density gradient (Ward-Thompson et al. 1999; Bacmann et al. 2000; Shirley et al. 2000, 2002; Evans et al. 2001; Young et al. 2003; Keto et al. 2004). Detailed observations of some individual dark clouds show density profiles that appear to match within a few percent those of pressure-confined, hydrostatic spheres (Bonnor-Ebert spheres; Bonnor 1956; Alves et al. 2001; Tafalla et al. 2004). While the observed morphologies of the starless cores are not always spherical and aspect ratios of 2:1 are common, the observed density profiles do not deviate significantly from those expected in near-equilibrium.

Radio-frequency spectral line observations that reveal the gas velocities within the cores confirm this near-equilibrium state. The observed spectral lines of all the starless cores are quite

[1] Harvard-Smithsonian Center for Astrophysics, 60 Garden Street, Cambridge, MA 02138.

narrow with no wings and nearly thermal widths, an indication that any gas velocities are a few tenths of the sound speed or less (Zhou et al. 1994; Wang et al. 1995; Gregersen et al. 1997; Launhardt et al. 1998; Gregersen & Evans 2000; Lee et al. 1999, 2001, 2004a; Alves et al. 2001; Keto et al. 2004). The cores contain a variety of gas motions: for example, contraction, expansion, or both within different regions of the core; but the observation that the gas velocities are all subsonic implies that the inertial forces are small and that there is near balance between the thermal and gravitational forces.

A state of near-equilibrium as indicated by both the dust and spectral line observations would allow the starless cores to be long-lived, apparently at odds with the transience required of the clouds in the theory of the turbulent interstellar medium. However, there might be no conflict between the two concepts of clouds as either transient entities or as pressure-supported dynamical units if the larger clouds are within and the starless cores are below the inertial range of the supersonic turbulence. The idea that the starless cores with their narrow line widths are clouds at the subsonic bottom of the turbulent cascade has been discussed in the literature since Larson's description of the size–line width relationship (Larson 1981; Padoan 1995; Goodman et al. 1998; Vázquez-Semadeni et al. 2003). What has evolved since the earliest description of the interstellar medium as a turbulent cascade is the concept of the larger scale clouds in the inertial range of supersonic turbulence as purely transient phenomena entirely out of equilibrium. The question now is whether all clouds in the interstellar medium, including the starless cores, are transitory.

We propose to test the hypothesis that the starless cores are clouds in quasi-equilibrium by comparing the predicted characteristics of model near-equilibrium cores against observations. If the modeled cores provide an adequate description of the observations, then we would conclude that quasi-equilibrium structures can and do exist in the interstellar medium. Given that the interstellar medium is dominated on larger scales by the structures of supersonic turbulence, then the starless cores must be the members at the bottom of the hierarchy, with scales below the sonic scale.

A similar approach of comparing model clouds in the turbulent hierarchy with observations was discussed in Ballesteros-Paredes et al. (2003). That research examined the density structures of a number of clouds produced in a numerical simulation of interstellar supersonic turbulence and compared their structures to the density profiles of pressure-supported, self-gravitating clouds. While none of the model clouds were in equilibrium, a number of them had density structures that matched those expected of clouds in equilibrium. Thus, one would conclude that observations of the density structure of clouds is an ambiguous test of their state of equilibrium. While that comparison was motivated by observations of the dust continuum in starless cores, an observation that typically provides only the density structure, there are many observations of molecular lines in starless cores that provide information on the velocity structure, the temperature, and the chemistry of the cores. With this additional information, the comparison is less ambiguous. For example, the clouds in Figure 9 of Ballesteros-Paredes et al. (2003) would never be confused with equilibrium structures because of the supersonic velocities within the model clouds. The dynamics of clouds with supersonic velocities are dominated by inertial forces and not their internal pressure. Therefore, "observations" of these model clouds that included spectroscopy would indicate that they cannot be in equilibrium.

Our research thus aims to reduce the ambiguity of the comparison by considering information that could be derived from molecular line observations of the starless cores in addition to the density structure derived from observations of the dust continuum. Since we model only individual clouds in quasi-equilibrium rather than the entire larger scale turbulent cascade, we can include in our models physics such as the radiative equilibrium of the dust and gas and the depletion of molecules from the gas phase by freezing onto dust grains that, with the present computing power, could not be fully incorporated into a three-dimensional hydrodynamic simulation. Finally, our models can be run at much higher spatial resolution. The level of detail provided by the additional physics and resolution improves the predictive power of our models and reduces the ambiguity of the comparison, allowing us to improve on the results of Ballesteros-Paredes et al. (2003).

The results of our comparison suggest that the observations of the starless cores are well explained by models in close equilibrium. For a given external pressure, the equilibrium may be stable or unstable to gravitational collapse, depending on the mass of the core. It seems reasonable to suppose that there will be a distribution in the initial masses of the cores because the cores are formed at the subsonic scale at the bottom of the turbulent cascade that itself follows a power-law distribution in size scale in the inertial regime. Cores that are more massive and dense at the time of formation ($n_{H_2} > 10^5$ cm^{-3} and a few $M_\odot$) will be ultimately unstable to gravitational collapse. Less dense examples may be in stable equilibrium, but stability does not imply that the cores must be static. For example, stable cores may oscillate in size and density around an equilibrium mean. While the unstable cores follow a progression toward greater densities and infall velocities, there is no evolutionary sequence linking the stable to the unstable cores. The less dense stable cores will not of themselves progress toward greater density and ultimate collapse, but may persist indefinitely until external conditions change. In this picture there are two classes of cores, and some of the inefficiency or slow rate of star formation is due to the formation of a significant fraction of the population of cores that are stable and not inclined to evolve to form stars.

2. PHYSICS OF THE STARLESS CORES

2.1. *Hydrostatic and Radiative Equilibrium*

Given the power-law relationship $\sigma_v \sim r^{1/3}$ between the turbulent velocity, σ_v, and the cloud length scale, r, the size scale where σ_v is the sound speed defines the fragmentation scale of the turbulent flow (Larson 1981; Padoan 1995; Goodman et al. 1998; Vázquez-Semadeni et al. 2003). Below this length scale, the turbulent velocities are subsonic, and the turbulent energy is less than the thermal energy. The fact that the thermal pressure dominates the dynamics immediately leads to a qualitative description of the structure of subsonic cores that matches the observed properties of the starless cores. Subsonic turbulence cannot produce substructure within the core, and therefore the density profile must be smooth and monotonic. Moreover, the density gradients must be characteristic of thermal pressure support, because the inertial forces are small unless the cores are in free-fall collapse. Thus, there must be approximate force balance, with thermal pressure rather than turbulent pressure as the dominant support against gravity.

If one imagines a boundary to the core, this leads to a description of the starless cores as hydrostatically supported spheres confined by an external pressure. If the gas is isothermal, these

spheres are generally referred to as Bonnor-Ebert (BE) spheres described by the solution of the Lane-Emden equation, truncated at some radius, with an external pressure that is set equal to the internal pressure, $P = nkT$, at the truncation radius (Bonnor 1956). Because the cores are embedded in larger scale molecular clouds, they are continuous with the surrounding molecular gas, with no sharp boundaries in pressure, temperature, or density. In particular, the notion of the starless cores as BE spheres does not require or imply a hot, rarefied interstellar medium around the cores. Because the velocity dispersion in the molecular clouds increases with the length scale, there is some scale around a core where the turbulence becomes supersonic, thermal pressure no longer dominates, and the dynamics are dominated by the inertial forces. This scale defines the boundary of the core. However, this definition is more conceptual than precise, and in practice, the boundaries in our models are chosen more simply; for example, to set the total mass of the core.

Whether a core in equilibrium can be long-lived depends on its dynamical stability against gravitational collapse. The gravitational stability of an isothermal sphere is described by Bonnor's criterion that the pressure at the boundary of the core should increase as the volume of the core is reduced. Similar to the case of an isothermal sphere, the static stability of a nonisothermal sphere, which might include some nonthermal internal pressure, can be determined by the sign of the change in boundary pressure as the volume of the core is reduced. Because the temperature variation in the starless cores varies by only several degrees around an average temperature of about 10 K, a stability analysis of the nonisothermal models shows a result that is similar to the isothermal case, although the critical values are somewhat different.

In § 3, we describe our static model for starless cores as spheres in hydrostatic and radiative equilibrium. This model serves as the starting point for the calculations of the hydrodynamic evolution, but it also provides a reasonable approximation to the internal structure of a starless core at any point in its evolution. This follows because the cooling time of a core is much shorter than its dynamical time and because the cores are always in near-equilibrium, unless they are in gravitational free fall. This will be justified later with the results of the evolutionary calculations.

3. MODELS OF HYDROSTATIC SPHERES IN RADIATIVE EQUILIBRIUM

The hydrostatic equilibrium is defined by the usual equations for the force balance between pressure and gravity, the mass of the sphere, and the equation of state (Chandrasekhar 1939):

$$\frac{dP}{dr} = \frac{GM(r)\rho}{r^2}, \tag{1}$$

$$\frac{dM}{dr} = 4\pi r^2 \rho, \tag{2}$$

$$P = kT\rho/m, \tag{3}$$

where m is the average mass per molecule, including helium and heavier elements. These equations are nondimensionalized by defining

$$\theta = T/T_R, \tag{4}$$

$$\sigma = \rho/\rho_c, \tag{5}$$

where ρ_c and T_R are a reference density and temperature. We use the density at the center of the sphere because the BE spheres are conventionally characterized by the central density, but we use the temperature at the boundary because the boundary temperature, unlike the central temperature, is nearly independent of the mass and density of the sphere. A linear scaling constant, a, related to the ratio of thermal to gravitational energy, is used to nondimensionalize the length and mass:

$$a = \left(\frac{kT_R}{Gm4\pi\rho_c}\right)^{1/2}, \tag{6}$$

$$\xi = r/a, \tag{7}$$

$$z = \frac{M(r)}{4\pi a^3 \rho_c}. \tag{8}$$

From the equations above, one derives two coupled ordinary differential equations, which we solve with a second-order Runge-Kutta algorithm, that define the density of a sphere in hydrostatic equilibrium for the temperature profile, θ, determined by radiative equilibrium:

$$\frac{dz}{d\xi} = \xi^2\sigma, \tag{9}$$

$$\frac{d\sigma}{d\xi} = -\frac{1}{\theta}\left(z\frac{\sigma}{\xi^2} + \sigma\frac{d\theta}{d\xi}\right). \tag{10}$$

Closely following several previous papers on the radiative equilibrium of the dark cloud cores, we calculate the radiative equilibrium of the gas assuming that the gas is heated by cosmic rays, cooled by molecular line radiation, and either heated or cooled by collisional coupling with the dust, depending on whether the dust is hotter or cooler than the gas (Larson 1973, 1985; Evans et al. 2001; Shirley et al. 2002; Zucconi et al. 2001; Stamatellos & Whitworth 2003; Gonçalves et al. 2004). For the dust,

$$\Gamma_{\rm ISR} - \Lambda_d = 0, \tag{11}$$

where $\Gamma_{\rm ISR}$ is the rate at which dust grains are heated by the external interstellar radiation field and Λ_d is the rate at which grains cool by blackbody radiation modified by the dust emissivity. The equilibrium gas temperature is defined similarly as the temperature at which the net gas cooling rate L is zero,

$$L = \Gamma_{\rm CR} - \Lambda_{\rm line} - \Lambda_{gd}, \tag{12}$$

where $\Gamma_{\rm CR}$ is the rate of heating by cosmic rays (eq. [13]), $\Lambda_{\rm line}$ is the rate of cooling by molecular line radiation (eq. [14]), and Λ_{gd} is the rate of energy transfer between the gas and the dust by collisions (eq. [15]). In equation (11), the lack of a corresponding term for the collisional coupling is an approximation reflecting the much higher rate of energy transfer by the dust through absorption and emission of radiation (Goldsmith 2001; Gonçalves et al. 2004). This allows the dust temperature to be calculated independently of the gas temperature. In equilibrium, the total radiative gas cooling rate $L = 0$, but during the hydrodynamic evolution, where the radiative gas cooling rate enters into the equation for the change in internal energy of the gas (eq. [20]), this rate is not generally zero, because the gas temperature is usually different from its value in radiative equilibrium because of compression or expansion of the gas.

The dust temperature at each point in the cloud is calculated by assuming radiative equilibrium between the incoming

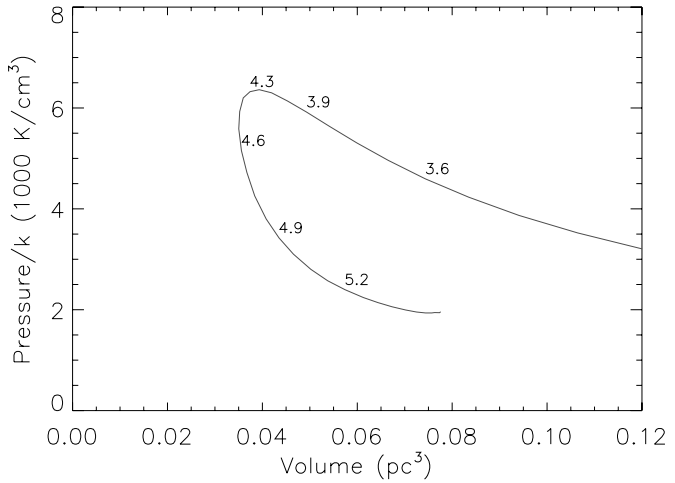

FIG. 1.—Curve of volume and boundary pressure of a 5 $M_\odot$ sphere in hydrostatic equilibrium and radiative equilibrium parameterized as a function of the gas density in the center of the sphere. The logarithm of the gas density is marked at points along the curve. The spheres are supported against gravity by the thermal pressure of temperatures ranging from 7 to 14 K. The spheres with central densities, volumes, and boundary pressures that are to the right of the maximum pressure are in stable equilibrium. Those spheres on the curve to the left of the pressure maximum are in unstable equilibrium. [*See the electronic edition of the Journal for a color version of this figure.*]

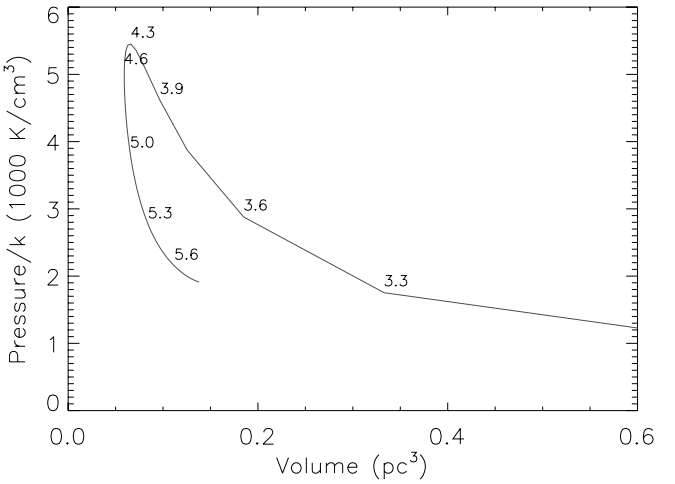

FIG. 2.—Same as Fig. 1, except that the sphere is isothermal at 10 K. [*See the electronic edition of the Journal for a color version of this figure.*]

interstellar radiation field that heats the dust and the infrared emission that cools the dust (Zucconi et al. 2001; Gonçalves et al. 2004). Our calculation uses the parameterization of the interstellar radiation field of Black (1994) and the parameterization of the dust opacities of Ossenkopf & Henning (1994) that are derived and described in Zucconi et al. (2001). The incoming interstellar radiation is attenuated by the overlying molecular gas, and the calculation of the incoming radiation field involves the optical depths from each point in the core to the surface of the core defined by the truncation radius for the nonisothermal BE sphere and averaged over rays at all angles. Because of the low temperatures in the cores, the dust radiates primarily in the far infrared, and the core is assumed to be transparent to this longer wavelength radiation.

Following Falgarone & Puget (1985) or Goldsmith (2001), we set the rate of energy transfer from cosmic rays into the gas as

$$\Gamma_{\rm CR} = 10^{-27} n_{\rm H_2} \text{ ergs cm}^{-3} \text{ s}^{-1}. \quad (13)$$

The molecular line cooling follows Goldsmith (2001) and uses the parameterized cooling functions for standard abundances that are derived in that study:

$$\Lambda_{\rm line} = \alpha (T_g/10 \text{ K})^{\beta} \text{ ergs cm}^{-3} \text{ s}^{-1}, \quad (14)$$

where the parameters α and β are given in Table 2 of Goldsmith (2001).

The parameterization is based on the large velocity gradient approximation, assuming a velocity gradient of 0.5 or 1.0 km s^{-1} pc^{-1}. In the model cores in our study, the velocity gradients are almost never this high. However, the large number of molecules with different abundances and transitions makes the parameterization insensitive to the exact velocity gradient. Molecular line radiation escapes the cloud, cooling the gas, through those transitions that have optical depths of approximately unity. As the density increases and the core becomes optically thick in a lower quantum transition of a more abundant species such as ^{12}CO (1–0), the radiation escapes through higher transitions of ^{12}CO and through transitions of less abundant species such as ^{13}CO. Thus, while the optical depth of one transition itself is a sensitive function of the assumed velocity gradient, the total cooling rate is a less sensitive function, since over a wide range of density and velocity gradient there are always some transitions of optical depth unity.

Energy is transferred between the gas and dust by collisional coupling. If we assume a Maxwellian distribution of random velocities in the gas (Burke & Hollenbach 1983) and a grain size distribution that we assume follows the -3.5 power of the grain radius from 0.03 to 0.3 μm (Krügel & Siebenmorgen 1994) and a gas-to-dust mass ratio of 100,

$$\Lambda_{gd} = 10^{-33} n_{\rm H_2}^2 T^{1/2} (T_g - T_d) \text{ ergs cm}^{-3} \text{ s}^{-1}. \quad (15)$$

This is essentially the same rate as was used by Zucconi et al. (2001), Goldsmith (2001), and Gonçalves et al. (2004).

Any two of the three parameters of central density, total mass, or external pressure along with a temperature profile is sufficient to specify the solution of the Lane-Emden equation for hydrostatic equilibrium. The temperature profile may then be determined for a given density profile by solving for the radiative equilibrium of the gas and dust. A few alternating solutions of the hydrostatic and radiative equilibrium equations result in a nonisothermal sphere characterized by a central density and total mass that is in equilibrium with an external pressure and interstellar radiation field.

3.1. *Results of the Static Modeling*

The stability of the nonisothermal cores is summarized in Figure 1 and compared to the stability of an isothermal core in Figure 2. In each figure, the equilibria on the curve to the left of the maximum equilibrium pressure are unstable to gravitational collapse. Because the central density correlates with the external pressure and inversely with the volume, the stability of a sphere can also be defined in terms of its central density. The curves in Figures 1 and 2 can be thought of as curves of equilibrium pressure and volume parameterized by density. Some representative central densities are plotted along the curves. A comparison of the curves shows that the critical boundary pressure or central density at which the equilibrium becomes unstable is different in the two cases, but the character of the curves is the same.

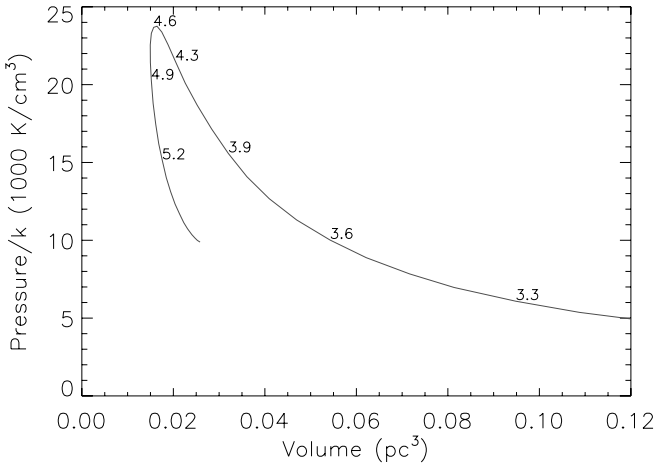

FIG. 3.—Same as Fig. 1, except that the gas has additional internal energy equal to one-quarter of the thermal energy. This additional energy could come from small-scale turbulence or magnetic fields. With this additional internal pressure, the clouds are able to support a higher maximum central gas density and boundary pressure. [*See the electronic edition of the Journal for a color version of this figure.*]

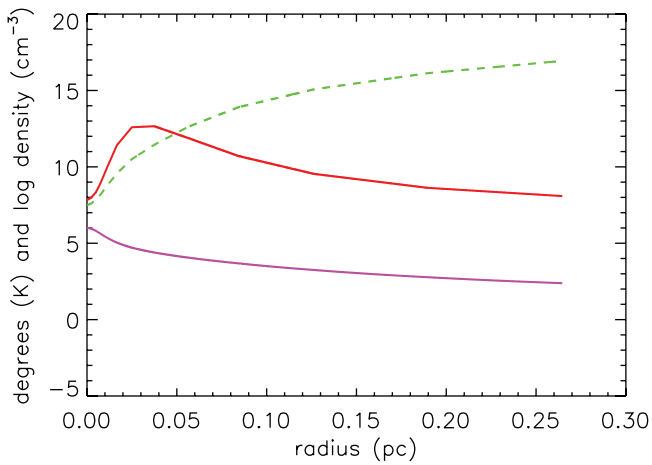

FIG. 5.—Same as Fig. 4, except that the central density of the sphere is 10^6 cm^{-3}. In this sphere the gas temperature initially increases inward as the molecular line radiation that cools the gas becomes ineffective because of the increasing optical depth. As the gas density increases to the critical density for gas-dust coupling, the gas temperature approaches the dust temperature. At the high gas density of this sphere, the sphere is unstable to gravitational collapse.

If the gas has additional internal energy, such as might be provided by small-scale subsonic turbulence or magnetic fields, the critical densities are higher. The stability diagram in Figure 3 shows the effect of additional internal energy equal to one-quarter of the thermal energy of the gas. The additional nonthermal energy improves the stability of spheres over their thermal counterparts.

The gas and dust temperatures and gas density for equilibrium spheres with central densities of 10^4 and 10^6 cm^{-3} are shown in Figures 4 and 5. These two densities lie on either side of the critical density for gravitational instability for a core with a total mass of 5 $M_\odot$. The figures illustrate the differences in structure predicted for stable and unstable cores. The most significant differences in the two cases are in the degree of central condensation and in the temperature.

The density profile of the unstable cores has a smaller radial width or higher degree of central concentration than that of the stable counterparts. In the observational literature, the width is usually defined as the radius of the central region of the observed core inside which the density is approximately constant and outside which the density falls as a power law. For example, the density profile may be described as $n \sim 1/(1 + r^\alpha)$ (Tafalla et al. 2004) or more simply in terms of two zones, an inner zone of constant density within a radius r_0 and a surrounding power-law envelope (Ward-Thompson et al. 1994). For cores with total masses of several $M_\odot$, the width of the constant-density region is about 2500 AU in the case of unstable prestellar cores and about twice that or 5000 AU in the stable starless cores.

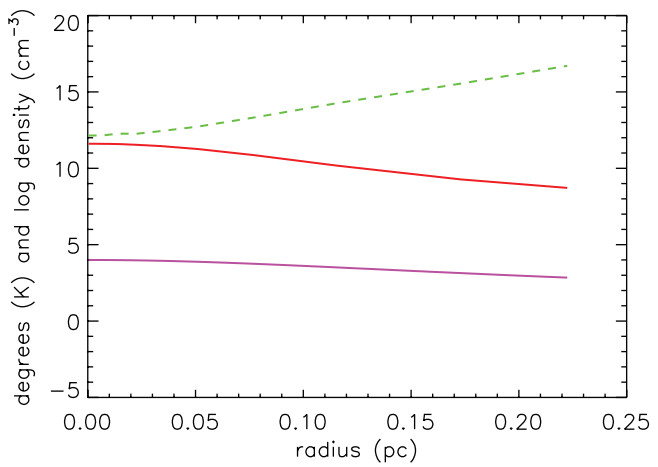

FIG. 4.—Dust and gas temperature and gas density as a function of radius for a sphere in radiative and hydrostatic equilibrium with a central density of 10^4 cm^{-3}. The logarithm of the gas density is shown by the lower line. The two upper lines represent the dust temperature (*dashed line*) and the gas temperature. The ordinate axis may be read as either the logarithm of the density in cm^{-3} or the temperature in units of K. The sphere is in stable gravitational equilibrium.

The gas temperature in a stable sphere with lower density is approximately constant at 10 K. Although the dust temperature decreases at smaller radii because the overlying cloud shields the dust in the center from external starlight, the gas and dust are not collisionally coupled, and the dust temperature has little effect on the gas. The gas cools primarily by molecular line radiation, and the increasing optical depth to line radiation causes a slight inward rise in temperature.

In the unstable core with high density, the increased optical depth to the external starlight reduces the heating of the dust. Because the dust is cooled by optically thin far-infrared radiation, the cooling rate remains constant, and the dust becomes colder toward the center. At central densities $>10^6$ cm^{-3}, the extinction through the core causes the dust temperature to decrease from 17 K at the boundary to below 8 K at the center.

The unstable core has a high enough density that the gas becomes optically thick to molecular line radiation and in addition begins to collisionally couple to the dust. Toward the center of the core, at densities $>10^5$ cm^{-3}, the gas and dust are collisionally well coupled and the gas is cooled predominantly through the dust. In the densest part of the unstable core, where the coupling is most efficient, the gas temperature approaches the dust temperature, around 8 K. Outside of the center, the collisional coupling and hence the gas cooling is reduced as the density decreases, and the gas temperature climbs to about 13 K. At still larger radii the optical depth to the surface of the core becomes low enough that the gas can cool efficiently through molecular line radiation, and the temperature falls to just below 10 K. The critical density of the nonisothermal cores in radiative equilibrium is above that of the 10 K isothermal core even though the central

temperature is lower in the nonisothermal core. This is because the cores in radiative equilibrium have a higher average temperature.

It is coincidental to the condition of radiative equilibrium that the densities at which the cores develop a strongly varying temperature profile are also the densities at which the cores become unstable to gravitational collapse. Nonetheless, this circumstance results in a useful division of the population of the starless cores into two classes. In the first category are cores that are true "starless" cores in that they will not of their own contract to form protostars. In the second category are "pre-protostellar" or "prestellar" cores that have not yet formed a protostar, but are unstable to collapse of the core and the formation of a protostar within a free-fall time. We combine the observational and theoretical descriptions and refer to the first category as stable starless cores and the second as unstable prestellar cores. In the absence of changing external conditions, there is no evolutionary path linking the two categories of cores. Stable cores do not evolve to become unstable.

3.2. *Comparison to Observations*

Examples of well-studied stable starless cores include B68 and L1517B. Well-known cores in the unstable prestellar category include L1544 and L1521F. Estimates of the central density in the stable starless core L1517B are 2.2×10^5 cm^{-3} from dust (Tafalla et al. 2004) and $10^{5.1\pm0.3}$ cm^{-3} from the molecular line N_2H^+ (Keto et al. 2004). The width of the density profile in L1517B is $35''$ (0.025 pc) from dust (Tafalla et al. 2004) and $0.022^{+0.008}_{-0.016}$ pc from N_2H^+. In the unstable prestellar core L1521F, the central density is estimated at 10^6 cm^{-3}, with a width of 0.017 pc for the central region of the core (Crapsi et al. 2004). The density structure of L1544 appears similar, with a central density of $10^{5.7\pm0.4}$ cm^{-3} and a width of 0.004 ± 0.002 pc from the observations of Keto et al. (2004) and 10^6 cm^{-3} with a width of $20''$ (0.015 pc) from the observations of Tafalla et al. (1998). In general, the stable starless cores have lower densities with broader density profiles than the unstable prestellar cores.

The theoretically predicted decrease in dust temperature has been observed in several cores. Infrared observations show a dust temperature profile that decreases from about 15 K at the edge of the core to 8 K in the center (Ward-Thompson et al. 2002; Pagani et al. 2003, 2004).

Molecular line observations of cores thought to be stable and not currently evolving toward star formation, such as L1517B and B68, show nearly constant gas temperatures with little variation across the core. Observations of L1517B in NH_3 indicate a gas temperature of 10 K (Tafalla et al. 2004), while observations of N_2H^+ indicate an average temperature of 9^{+7}_{-2} K (Keto et al. 2004). Temperature estimates of B68 range from 10 to 16 K (Alves et al. 2001; Lada et al. 2003).

Observations of the core L1544 indicate an average temperature of 8.75 K (Tafalla et al. 1998) from NH_3 lines and 11 ± 4 K (Keto et al. 2004) from N_2H^+, both consistent within the observational uncertainties with the models, but the spectral line observations do not have the angular resolution or the sensitivity to define the temperature profile of the gas with the detail of the models. In general, temperature estimates of the stable starless cores are a few degrees warmer than those of the unstable prestellar cores, consistent with the higher temperatures predicted by the models.

In order to understand the velocity structure of the cores and to interpret spectral line observations, it is necessary to model the hydrodynamic evolution of the cores. In §§ 4 and 6, respectively, we develop the hydrodynamic model and present some examples of the evolution of cores. We find that both classes of cores, stable starless and unstable prestellar, may have coherent internal velocities. The stable starless cores can exhibit a variety of oscillatory motions, expansion and contraction, that do not result in the collapse or dissipation of the core. The unstable prestellar cores have inward velocities that ultimately evolve to gravitational collapse at free-fall velocities. The two types of cores can be distinguished by their spectral line profiles and widths. The spectral lines of unstable prestellar cores tend to show strongly asymmetric profiles split by self-absorption. Also, the spectral line widths of volatile molecular species are broader in the unstable prestellar cores than they are in the stable starless cores.

4. HYDRODYNAMIC MODEL

To model the evolution of the starless cores, we use a simple one-dimensional hydrodynamic code with a first-order Lagrangian discretization and Richtmyer–von Neumann pseudoviscosity. While this method is not as sophisticated as the piecewise parabolic method (PPM; Colella & Woodward 1984) used in one of the previous dynamical studies of BE spheres (Foster & Chevalier 1993), the improvement in computer speed allows our hydrodynamic code to be run with a factor of 10 more grid points than in that previous study, and this allows better spatial resolution despite the inherent smoothing in the pseudoviscosity method. Also, in our study the resolution is not as important as in the Foster & Chevalier study. First, our investigation concerns only the stability of starless cores. Thus, we follow the evolution of cores only to a scale of AU, which is sufficient to determine the stability and evolutionary path of the core. For the typical conditions in starless cores, most of the velocities are subsonic on this scale. In contrast, the previous calculations of Foster & Chevalier also sought to characterize the asymptotic behavior of the flow at the time of formation of a point source at the flow center. Near a gravitational point source, the flow can accelerate to arbitrarily high Mach numbers. In contrast, to determine the fate of a core, our simulations need not follow evolution much past the point when the flow has accelerated to more than unity Mach number. Supersonic infall velocities imply that the core is in free-fall collapse, and its fate is sealed.

The typical core size in our models is 0.2 pc. The grid is initially linear with approximately 5000 points, yielding a resolution of about 10 AU. The sound speed is about 0.2 km^{-1}, so the Courant condition implies a maximum time step of about 250 yr. The simulations are run with a time step of 1/10 the maximum indicated by the Courant condition, initially about 25 yr. At the end of the evolution of an unstable core, the typical maximum spatial resolution in the center of the core is less than 1 AU, with a time resolution of less than 1 yr. As will be discussed below, the limiting resolution in these simulations is not that of the hydrodynamics, but of the radiative transfer.

The hydrodynamical equations in Lagrangian form are

$$r(s, t) = s + \int_0^t v(s, t)\, dt, \tag{16}$$

$$\frac{1}{\rho(r, t)} = \frac{1}{\rho(s, 0)} \left[\frac{r(s, t)}{s}\right]^2 \frac{\partial r}{\partial s}, \tag{17}$$

$$P(r, t) = \rho(r, t) kT/m, \tag{18}$$

$$\frac{\partial v}{\partial t} = -\frac{1}{\rho(s, 0)} \left[\frac{r(s, t)}{s}\right]^2 \frac{\partial (P + q)}{\partial s} - \frac{GM(r)^2}{r}, \tag{19}$$

$$\frac{\partial E}{\partial t} = \frac{P + q}{\rho} \frac{\partial \rho}{\partial t} - \frac{L}{\rho}. \tag{20}$$

In these equations, s is the original position of each Lagrangian cell, $r(s, t)$ is the corresponding position at time t, $M(r)$ is the mass contained within radius r, E is the internal energy of the gas, L is the radiative gas cooling rate defined in equation (12), and q is the Richtmyer–von Neumann pseudoviscosity

$$q = \begin{cases} l^2\rho[\partial v(s, t)/\partial s]^2 & \text{when } \partial v/\partial s < 0, \\ 0 & \text{when } \partial v/\partial s > 0, \end{cases} \quad (21)$$

where l is a constant that is approximately the shock smoothing width over the grid spacing. These equations are discretized as in Richtmyer (1957).

In our calculations of the hydrodynamic evolution of the cores, we start with a core in hydrostatic equilibrium and in radiative equilibrium. In the subsequent hydrodynamic evolution, the temperature of the gas is calculated at each time step, taking into account the $P\,dV$ work of compression or expansion and the rate for radiative cooling, L (eq. [12]). Using the parameterized approximations for the gas cooling, the change in internal energy may be calculated for each grid cell using only the local values of density and velocity (compression) of the gas and the temperatures of the gas and dust. The dust temperature itself depends on the global structure of the core: the angle-averaged optical depth to the surface from each radial point. However, because the larger scale structure of the core changes relatively slowly compared to the time step of the hydrodynamic evolution, set by the Courant condition, the angle averaging to determine the dust temperature need not be computed at every time step. In addition, because of the approximation that the dust temperature is set only by the radiative equilibrium of the dust and is independent of the gas temperature, the dust temperature must be a smoothly varying function in the core. Thus, the dust temperature can be computed less frequently and on a coarser grid and interpolated onto the hydrodynamic grid.

The initial core always contains some perturbations that cause some initial movement of the gas in the core. These perturbations, at a fraction of a percent level, are primarily due to coarse gridding of the dust equilibrium and are on the scale of the coarse grid, about 1/20 of the size of the core. The perturbations arise because the initial dust and gas temperatures exactly match conditions of hydrostatic and radiative equilibrium on the coarse grid, but the interpolated dust temperatures and thus the interpolated gas temperatures do not exactly match the gas temperature required for hydrostatic equilibrium between grid points. In both stable and unstable clouds, the perturbations are smoothed in a timescale of $\delta/c_s \sim 10^4$ yr by small changes in temperature and density that quickly establish radiative and hydrostatic equilibrium. In the gravitationally stable clouds, once the perturbations are smoothed out, no further evolution takes place. In gravitationally unstable cores, even though the initial perturbations are quickly smoothed, the core is unable to establish an exact equilibrium, and after a long time, several sound crossing times or tens of free-fall times, the core will begin gravitational collapse. The length of time for the core to begin collapse is simply the time required for very small perturbations to reach any appreciable magnitude. Once the inward velocities reach even a few hundredths of the sound speed, the core collapses in about a free-fall time, $t_{\rm ff} \sim (G\rho)^{-1/2} \sim 10^5$ yr. Were it not for these perturbations deriving from the coarse gridding of the radiative transfer, it would be necessary to introduce perturbations into the initial structure so that the unstable cores would collapse before patience with the hydrodynamic evolution was exhausted.

5. RADIATIVE TRANSFER AND CHEMISTRY

After the numerical hydrodynamic evolution of the cloud has been completed, the temperature, density, and velocity as a function of time are transferred to a non-LTE accelerated Λ-iteration (ALI) radiative transfer code to determine model spectral line profiles for comparison with observations (Keto et al. 2004). The model cores are assumed to be at 150 pc, the distance to the Taurus star-forming region, and to be observed with a telescope with a beam width of $20''$. Because the core radii are on the order of 10 beams, the resolution is not critical except in the cases of the unstable cores that have rapidly increasing density and velocity gradients in their centers.

To compute the spectral line profiles, we also need to know the abundances of the molecules, in addition to the information provided by the hydrodynamical evolution. The gas-phase abundances of molecules are variable within the core, because in the cold dense interiors of the dark cloud cores, molecules freeze out of the gas phase onto the surfaces of dust grains at different characteristic densities according to their different volatilities (Brown et al. 1988; Willacy & Williams 1993; Hasegawa et al. 1992; Hasegawa & Herbst 1993; Caselli et al. 1999, 2002a, 2002b, 2002c; Bergin et al. 1995, 2002; Tafalla et al. 1998; Aikawa et al. 2001). We follow Bergin et al. (2001) and Tafalla et al. (1998, 2004) and approximate the dependence of the abundance on the density n as an exponential:

$$X(n) = X_0 \exp(-n/n_d), \quad (23)$$

with parameters for CS of abundance $X_0 = 10^{-8}$ and density $n_d = 10^4$ cm^{-3}. A more complete treatment of the molecular abundances of the starless cores derived from detailed chemical modeling is discussed in Lee et al. (2004b). That study concludes that a simple parameterized model of depletion, as adopted in our simulations, is a reasonable approximation to their more detailed analysis.

6. MODEL CORES

We adopt as a standard model a core with a total mass of 5 $M_\odot$ and consider its evolution under a variety of conditions that could be expected in and around the dark cloud cores. For a given mass, the central density determines the gravitational stability of a nonisothermal BE sphere. We model the evolution of cores with a range of central densities $n_{\rm H_2} = 10^3$–10^7 cm^{-3} centered around the critical density for gravitational instability, approximately $n_{\rm H_2} \sim 10^4$ cm^{-3} for a core of 5 $M_\odot$.

A core could be subject to a variation in external pressure from a nearby supernova, bipolar outflow, or the turbulence of the interstellar medium. A change in external pressure could cause oscillations in a core, and a sufficient increase in external pressure could cause a previously stable core to collapse. Accordingly, we model the evolution of some cores in response to changing external pressure.

The dark cloud cores may have some component of magnetic or turbulent support in addition to thermal support. In a one-dimensional model, this additional support can be approximated by modifying the equation of state to include a nonthermal pressure. This assumes that the nonthermal or magnetic energy has a characteristic scale much smaller than the core so that the effect is at least approximately the same as an isotropic pressure. This assumption follows from estimates that show that the large-scale magnetic fields in cores are too weak to affect their evolution (Nakano 1998). Thus, we may assume that the nonthermal pressure is small-scale and isotropic. If the nonthermal pressure

is initially proportional to density, then the initial structure of the core may be determined as before with the Lane-Emden equation, but with a higher effective temperature than in the case of support only through thermal pressure. The subsequent evolution of the core depends on the equation of state of the nonthermal pressure. For example, the cores that we modeled with a nonthermal adiabatic index greater than 4/3 behave as expected and never collapse to a point source, but form an inner core of approximately constant density supported by nonthermal pressure. As the core evolves, the surrounding envelope continues to collapse onto this inner core, creating a steep density gradient and shock at the boundary of the inner core. Such a boundary region is never seen in observations of dark cloud cores, suggesting that the molecular gas in the dark cloud cores must have a lower value of the adiabatic index. In an analysis of the virial theorem, McKee & Zweibel (1995) suggested that the adiabatic index for magnetic turbulence should be between 3/2 and 1/2, depending on the time and length scales of the turbulence. A particularly convenient choice is an adiabatic index of unity. This of course matches the adiabatic index of the thermal pressure, and the dynamics are therefore similar to a thermally supported core with a higher temperature. However, the nonthermal pressure remains proportional to density only, while the thermal pressure, being proportional to the temperature as well as the density, changes as the temperature is changing.

We ran about 30 different numerical simulations to explore different combinations and ranges of parameters. Densities considered in our study include those

1. expected to be stable;
2. near the critical density of the nonisothermal BE sphere;
3. expected to be unstable.

Different equations of state considered in this study are those with

1. thermal pressure only;
2. thermal pressure with a nonthermal pressure initially proportional to density:

a) an adiabatic index of nonthermal pressure equal to unity;
b) an adiabatic index of nonthermal pressure equal to 4/3.

Different external conditions applied to the cloud were

1. constant external pressure;
2. increasing external pressure:

a) external pressure remaining below the critical pressure of the nonisothermal BE sphere;
b) external pressure sufficiently high to cause collapse.

Hydrodynamic models were computed for combinations of all the cases above. Despite the variety of initial conditions and equations of state, the behavior and properties of the stable starless cores are quite similar to each other, as are the behavior and properties of the unstable prestellar cores. In §§ 6.1 and 6.2, we discuss in detail two models to illustrate the characteristics of the two classes of cores. We model the unstable prestellar cores with a hydrodynamic simulation that starts from an initial configuration in unstable equilibrium and evolves toward free-fall gravitational collapse. The stable starless cores are modeled with a simulation that starts in stable equilibrium and is perturbed into oscillatory contraction and expansion by a sudden increase in the external pressure. Finally, in order to illustrate the thermal instability that is related to the critical density for gas-dust collisional coupling, we discuss the evolution of a core with an initial configuration that is both gravitationally and thermally unstable. The initial expansion of this core caused by the thermal instability results in a stable core undergoing damped oscillations of expansion and contraction.

6.1. *Hydrodynamic Evolution of an Unstable Pre-Protostellar Core*

The theoretical evolution of a gravitationally unstable core is dynamically as expected from previous simulations: small numerical perturbations grow for several crossing times (several Myr) until they are sufficient to tip the core off its initial unstable equilibrium toward collapse (Hunter 1977; Foster & Chevalier 1993). Since the cooling time is short compared to the dynamical time, the temperature profile is set almost entirely by radiative equilibrium. Figures 6–8 show the properties of the core as the collapse proceeds. Also shown are accompanying molecular line spectra as would be observed toward the center of the core.

Figures 6–8 show that the approximate force balance between pressure and gravity that is set in the initial configuration is maintained until the infall velocities begin to approach the sound speed. Thus, the density structure continues to approximate that of a pressure-supported BE sphere as the core evolves toward free-fall collapse.

Our hydrodynamic simulation, as well as analytic considerations (Whitworth & Ward-Thompson 2001), show that gravitational collapse starting from an equilibrium-configuration BE sphere is characterized by inwardly increasing velocities. A velocity profile with velocities that increase inward is not unique to the density profile of unstable BE spheres but is still a diagnostic inasmuch as other initial configurations such as the uniform spheres considered in Jeans instability and the well-studied singular isothermal spheres (Shu 1977) and singular logotropic spheres (McLaughlin & Pudritz 1997) evolve to collapse with very different velocity profiles. Inwardly increasing velocities are indicated in molecular line observations of the cores L1544 and L1521F by the velocity gradient inferred from the details of the observed spectral line shapes and from the widths of spectral lines of volatile molecular species that increase toward the centers of the cores. Figures 6–8 show how the spectral profile of N_2H^+ develops the characteristic asymmetric split with a stronger blue peak as the infall velocity increases. This characteristic split is seen in the observed N_2H^+ spectrum from L1544; for example, in Figure 2 of Williams et al. (1999) and in Figures 4 and 5 of Keto et al. (2004). An increase in the line width of N_2D^+ is observed toward the centers of the cores L1544 and L1521F (Caselli et al. 2002c; Crapsi et al. 2004, 2005). Although the observations of line width do not indicate the direction of the velocity, the increase in line width is indicative of an increase in the magnitude of the velocity toward the center of the core.

6.2. *Hydrodynamic Evolution of a Stable, Oscillating Starless Core*

Hydrodynamic simulations of cores in stable equilibrium show no evolution unless the core is subjected to a perturbation. While observations of many cores do not show velocities above the observational detection limit, about 1/10 of the sound speed, other cores indicate expanding or contracting motions or more complex combinations indicative of nonspherical perturbations. While some of these cores may be unstable and evolving toward collapse as described in § 6.1, others may be oscillating around an equilibrium mean. The nonspherical morphologies of many cores, often showing aspect ratios of 2:1, may indicate

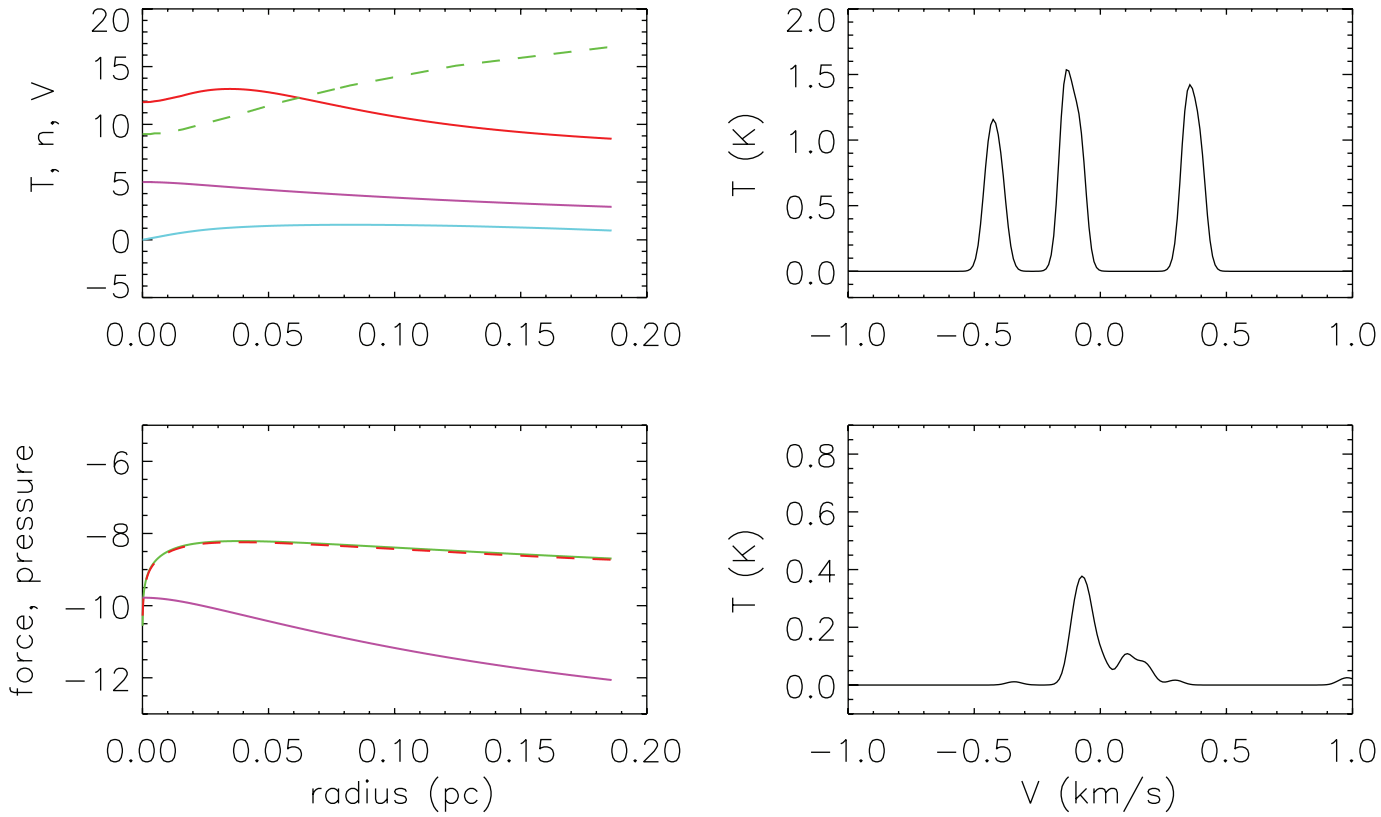

FIG. 6.—Evolution of a core starting from an initial configuration that is in equilibrium but unstable to gravitational collapse. In this simulation, the cloud remains static for about 3 Myr, about 3 sound crossing times, while small perturbations originating from numerical noise build up to move the cloud off its unstable equilibrium. Once the cloud begins to contract, the velocities in the center of the cloud become supersonic in a few 10^5 yr and the core is then in unsupported free fall. *Top left*: Density (log cm^{-3}) and gas and dust temperatures (K), in the same format as Figs. 4 and 5, and also the velocity (sound speed times -10) as a function of the radius (pc). For example, a velocity of 10 on the left axis indicates an inward velocity equal to the sound speed. *Bottom left*: Gravitational force (*solid green line*), pressure force (*dashed red line*), and pressure (*solid purple line*), in cgs units. This panel (in the subsequent figures) shows that the cloud remains in approximate force balance until the core begins free-fall collapse. *Right*: Spectral lines of N_2H^+ (1–0) and N_2H^+ (3–2), as they would be observed in the model core. The radiative transfer simulation assumes that the core is at a distance of 150 pc and that the telescope beam is 20″. Each panel shows the hyperfine lines that are within ± 1 km s^{-1}. These are the inner three hyperfines in the case of N_2H^+(1–0).

oscillations about an equilibrium mean that may be stable or unstable.

In our example model of a stable starless core, we begin the hydrodynamic simulation in hydrostatic and radiative equilibrium. The core starts with a central density of 2×10^3 cm^{-3}, well to the stable side of the Bonnor criteria for nonisothermal spheres, so an increase in external pressure by a factor of 1.5, held constant thereafter, pushes the core close to but not past the maximum pressure for stability. The increase in pressure propagates into the core, eventually reflecting off the center, while the core as a whole adjusts its density profile to a new equilibrium with the increased external pressure. An initial overshoot of the new equilibrium results in damped oscillations of contraction and expansion. The oscillations imply that inertial forces are important in the dynamics, but the inertial forces are still small compared to the pressure and gravitational forces, so the core remains in approximate force balance throughout the evolution.

Figure 9 shows the structure of the core and the accompanying spectra when the head of the velocity and pressure wave has advanced halfway into the cloud at elapsed time 1.003 Myr. Because of the low density, the gas cools efficiently throughout the volume of the cloud by molecular line radiation, and the gas temperature is nearly constant. The predicted spectral line profiles of an oscillating core are particularly interesting in comparison with observed profiles. The CS (1–0) spectrum shows an asymmetric profile with a stronger blue peak that is characteristic of inward motion. In Figure 10, at 1.613 Myr, the wave has reflected off the core and is headed outward. At this time, most of the core is still moving inward, responding to the increased external pressure, and the spectral line profile of CS still shows an asymmetric line split characteristic of inward motion. By a time of 3.705 Myr (Fig. 11), when the contraction of the core has overshot the equilibrium point, the whole core is expanding outward. The spectral line profiles of CS now show an asymmetric split line with a stronger red peak that is characteristic of outward motion. Observations of CS spectra in B68 show asymmetric split spectra of both senses, inward motions and outward motions, at different positions in the cloud; see, for example, Figure 6 of Lada et al. (2003).

Model spectra of N_2H^+ from the same hydrodynamic simulation show only symmetric profiles with no asymmetric splitting. The difference between the CS spectra and the N_2H^+ spectra relates to the differences in the velocity fields in the regions where each of the molecular lines is generated. In the dense centers of the starless cores, the CS molecule is depleted from the gas phase by freezeout onto dust grains, but the more volatile N_2H^+ molecule maintains a constant abundance. Because the line brightness for any subthermally excited molecule scales with the square of the density, the N_2H^+ line is formed predominantly in the dense gas in the center of the core, whereas the CS line is

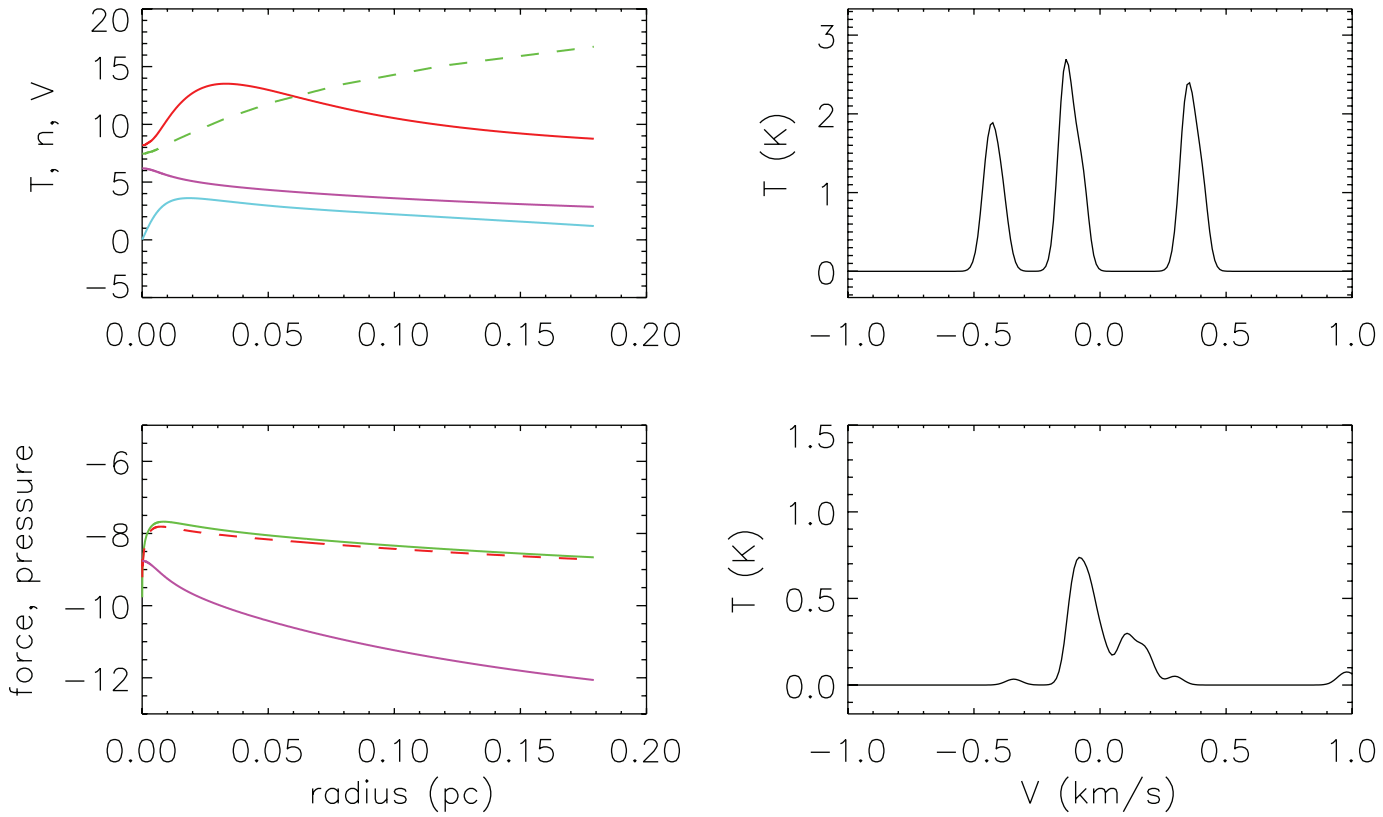

FIG. 7.—Same as Fig. 6, but at an evolutionary time of 3.22 Myr. As the gas density in the center increases, the gas becomes collisionally coupled to the dust and the gas temperature approaches the dust temperature.

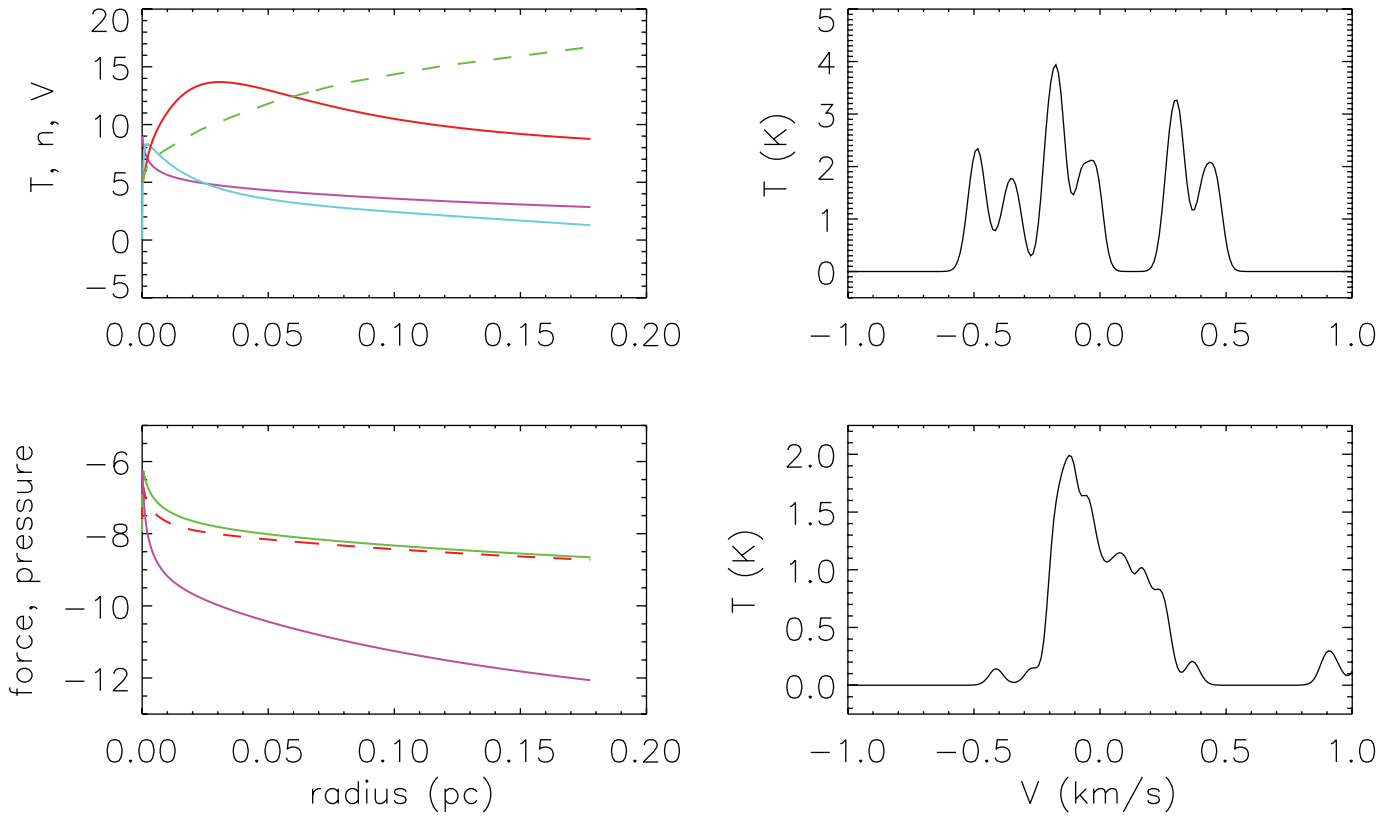

FIG. 8.—Same as Fig. 6, but at an evolutionary time of 3.37 Myr. As the velocity gradient steepens, with the inward velocity approaching the sound speed in the center of the cloud and the velocities still near zero at the edge, the low-velocity gas at the edge of the cloud absorbs the emission from the center of the cloud, creating a split spectrum. The profile of the N_2H^+ (3–2) line is dominated by numerous hyperfine components.

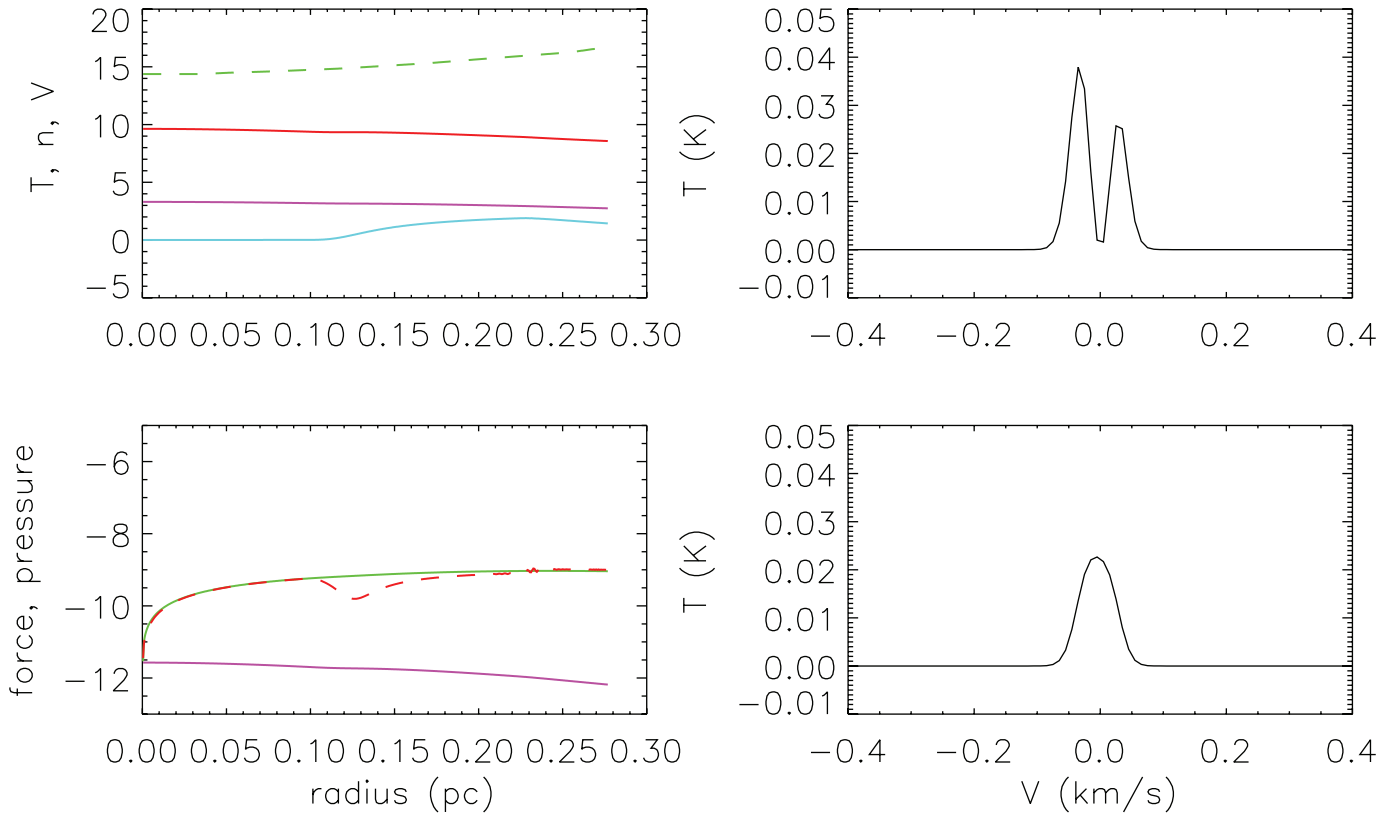

FIG. 9.—Evolution of a core starting from an initial configuration that is in stable equilibrium but subject to an increase in the external pressure by a factor of 1.5. In this simulation, the core contracts to a new equilibrium configuration in response to the increased pressure through damped oscillations of contraction and expansion. This plot shows the model at an evolutionary time of 1.003 Myr, when the pressure wave has moved about halfway into the core. The four panels are as explained in Fig. 6, except that the spectral lines illustrated in this figure are CS (1–0) and CS (3–2). The asymmetric and split CS (1–0) spectrum with the brighter blue peak is indicative of contraction. The CS (3–2) line does not show this splitting because the line is optically thin.

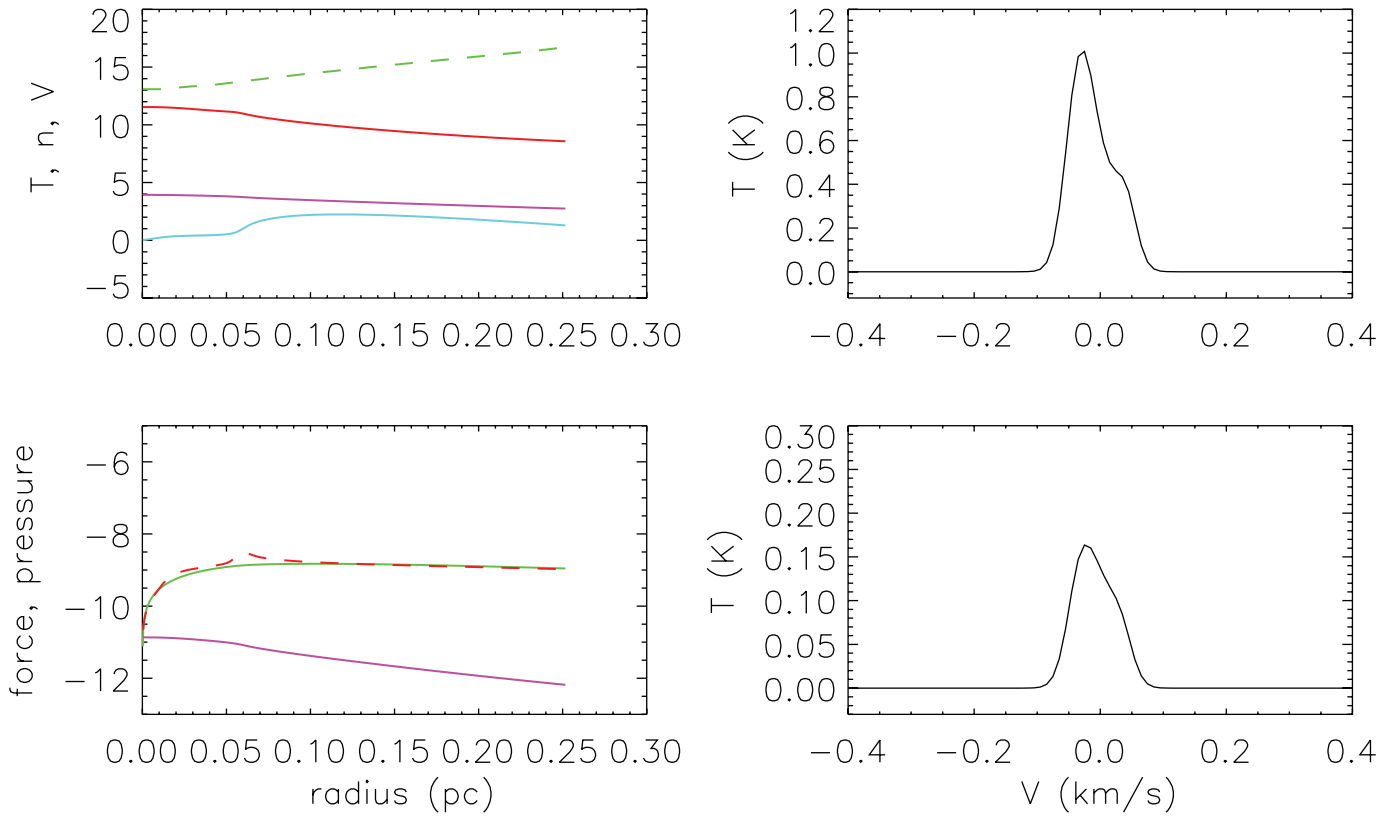

FIG. 10.—Same as Fig. 9, but at an evolutionary time of 1.613 Myr, when the pressure wave has reflected off the center of the core. Even though the pressure wave is moving outward, most of the cloud is still contracting in response to the increased boundary pressure, and the asymmetric CS spectra show a brighter blue peak indicative of contraction. The CS (3–2) spectrum shows asymmetry because at the higher gas density, the line is becoming optically thick.

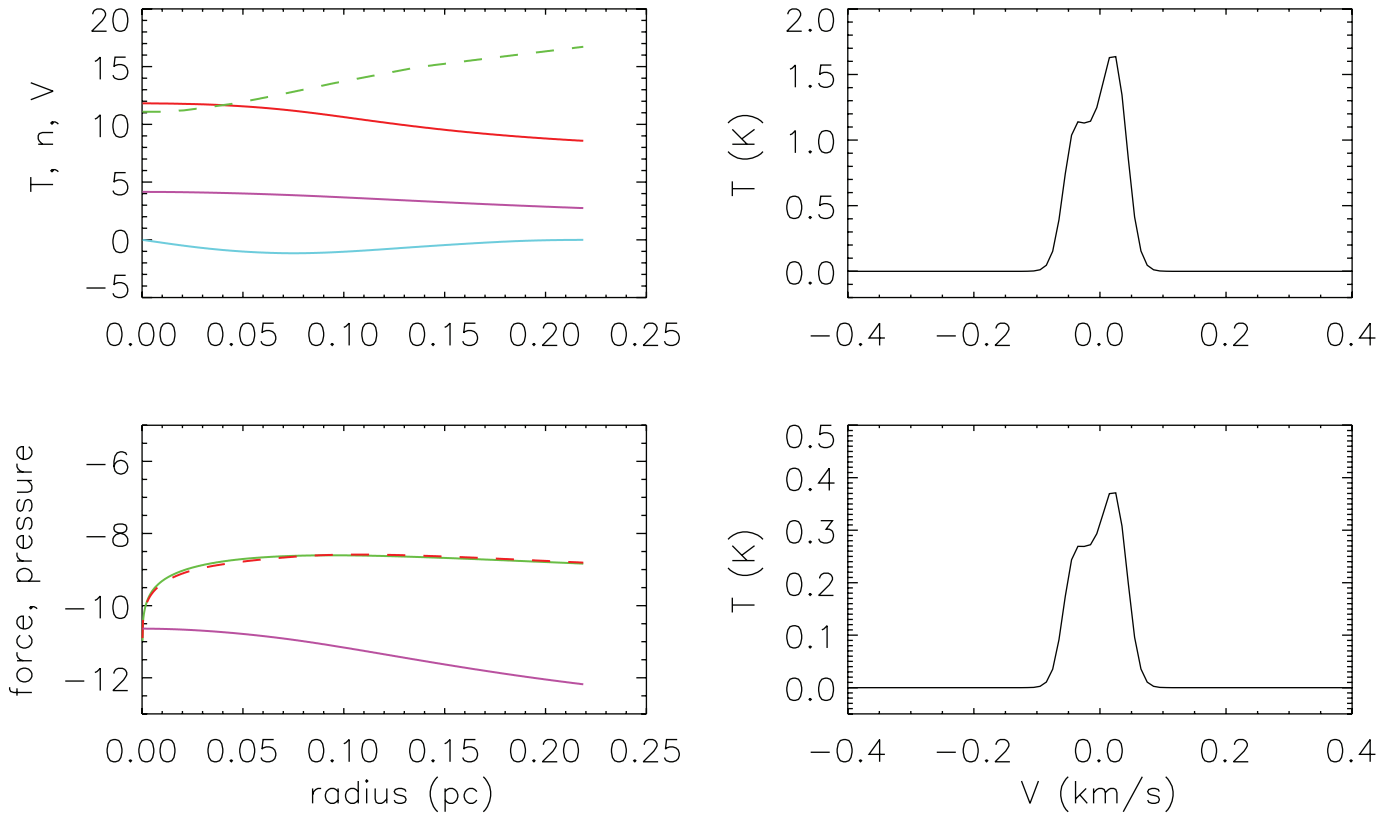

FIG. 11.—Same as Fig. 9, but at an evolutionary time of 3.705 Myr. At this time most of the cloud is expanding, having overshot the equilibrium with the increased external pressure. The asymmetric CS profiles now show a brighter red peak indicative of expansion.

formed predominantly in the envelope. In the breathing-mode oscillations such as those induced in our simulation by an increase in the external pressure, the highest velocities are generally found in the envelope, while the velocity in the core remains low. Thus, the theoretical model indicates that the CS molecule will show an asymmetric split spectrum, while the N_2H^+ molecule will not.

The theoretically predicted line shapes of the volatile and depleting species are observed in L1517B. Observations of N_2H^+ in L1517B, Figure 13 of Keto et al. (2004) and Figure 6 of Tafalla et al. (2004), show only narrow symmetric spectra, while the spectrum of HCN (another species strongly depleted in dense gas) shows a pronounced asymmetric split with a higher blue peak indicating expansion (Sohn et al. 2004). On the basis of the modeling, L1517B would be in the expanding phase of an oscillation. Observations of B68 in N_2H^+ and CS also match the theoretical prediction, with a nearly symmetric profile observed in the volatile N_2H^+ molecule and significant splitting observed in the more refractory tracer; for example, Figure 2 of Lada et al. (2003) and in Redman et al. (2005).

In general, the stable starless cores show warmer temperatures, lower densities, less central concentration of their density profiles, and a variety of spectral line shapes, including both expansion and contraction. Since the velocities in the centers of the stable starless cores are very low, the spectra of volatile tracers show no increase in line width at positions closer to the core center. In contrast, the increased line widths of volatile tracers observed toward the centers of unstable prestellar cores have much higher velocities in their centers than in their envelopes. This combination of properties is sufficient to distinguish these cores that are not currently evolving to form protostars from those in the unstable category that are in the earliest stages of protostellar formation.

6.3. *A Thermally Unstable Core*

Under the right conditions, a core may be subject to a thermal instability if as the core expands, the collisional coupling that allows the dust to cool the gas is reduced, causing the gas to warm and further drive the expansion. Since the gravitational stability is determined by the total mass of the core, as well as the density, while the gas-dust collisional coupling is a function of the density alone, a core may be unstable to gravitational collapse but thermally unstable to expansion. As a last example, we follow the evolution of a model core whose initial configuration is doubly unstable.

The central density in the initial equilibrium configuration is 10^5 cm^{-3}, placing it on the gravitationally unstable portion of the Bonnor stability curve in Figure 3. However, because the density is very close to the critical density for the collisional coupling of the gas and dust, the core is thermally unstable to expansion. As the core expands, the cooling of the gas is reduced as the transfer of energy from the gas to the dust through collisions becomes less effective. The gain in internal energy, dQ/dt, then furthers the expansion. The increase in energy from the reduced cooling is related to the gas temperature and the work done in expansion,

$$\frac{dQ}{dt} = \frac{d}{dt}\left(\frac{3kT}{2m}\right) + P\frac{dV}{dt}. \tag{24}$$

The numerical simulation (Fig. 12) shows that as the cloud expands, the gas temperature increases, while the density (volume^{-1}) decreases. This is seen in the first cycle of expansion, which occurs at times less than 2 Myr and for densities less than $10^{4.5}$ cm^{-3}, when the temperature increases with decreasing

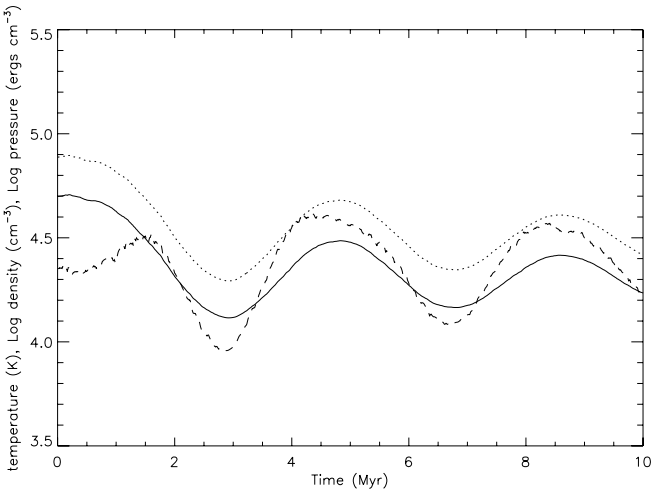

FIG. 12.—Temperature, density, and pressure as a function of time at the center of a core with an initial configuration that is unstable to gravitational collapse and also unstable to expansion by a thermal instability. The thermal instability is evident in the early evolution of the cloud, where the temperature can be seen to be increasing as the density decreases. Once the cloud has expanded so that the density remains below the critical density for gas-dust coupling, the thermal instability no longer operates and the temperature behaves as for a gas with an approximately adiabatic equation of state. The logarithm of the gas density (cm^{-3}) is shown by the solid line, the logarithm of the pressure (ergs cm^{-3}) is shown by the dotted line, and the temperature is shown by the dashed line. To align the curves vertically, 7 has been subtracted from the temperature and 1 from the log pressure.

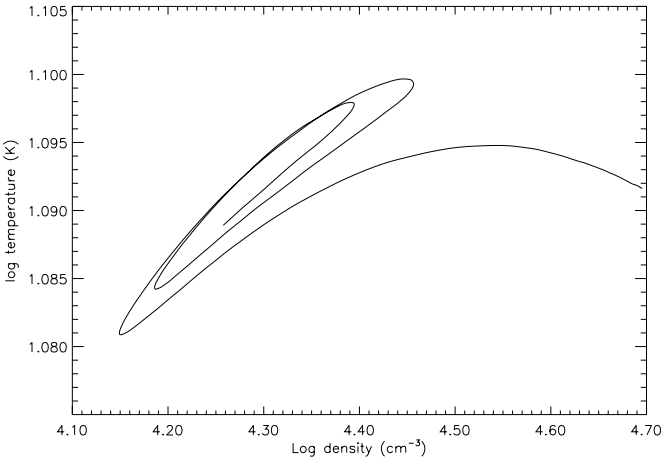

FIG. 13.—Temperature vs. density at all times during the evolution of the thermally unstable core with the evolution illustrated in Fig. 12. The slope of the curve is the effective adiabatic index of the gas, $T \sim \rho^{\gamma-1}$. The effective adiabatic index, given by the slope of the curve plus unity, evolves from negative to positive as the cloud expands.

density, the opposite of the behavior expected for a gas with an adiabatic equation of state. After this time, the density is low enough that the gas is no longer collisionally coupled to the dust, and the gas behaves approximately adiabatically, with the temperature and density increasing or decreasing together.

The core resolves its doubly unstable state by expansion to a lower density state that is both gravitationally and thermally stable. Expansion is favored over collapse in this model core, even though the linear analysis of Field (1965) predicts that both expansion and contraction are equally unstable as long as the perturbations are small. Although the linear thermal instability itself is symmetric, in the model core the asymmetry toward expansion derives from nonlinear effects associated with the radiative equilibrium of the dust. For example, in the initial state of the model, the gas is collisionally well coupled to the dust, and the temperatures of the gas and the dust are nearly the same. An increase in density does not cause the gas to become cooler because increased collisional coupling cannot reduce the gas temperature below the dust temperature. The dust temperature remains approximately constant because density changes localized in the center of core do not significantly affect the overall radiative equilibrium and temperature. On the other hand, a decrease in the gas density in the center of the core causes an immediate increase in the local gas temperature because of the reduced collisional coupling. Thus, the instability appears one-sided.

The thermal instability is also evident in the variation of pressure with temperature and density. For an adiabatic change, the three quantities are related as $P = k\rho^{\gamma}$ and $T = k\rho^{\gamma-1}$, where γ is the ratio of specific heats and k is a constant. A plot of the logarithm of the temperature as a function of the logarithm of the density (Fig. 13) shows that at low density the slope of the curve is negative. If the relationship between T and ρ were expressed in the form of the adiabatic relationship, then $\gamma' < 1$, where γ' is the exponent derived from the empirical relationship between T and ρ rather than the ratio of specific heats, as in the adiabatic relationship. However, on the portion of the $\log T$ versus $\log P$ curve corresponding to the initial stage of the expansion when the gas is at higher density, the slope of the curve is positive, and γ' must be greater than unity. A corresponding plot of the gas pressure versus density would show that γ'' in the relationship $P \sim \rho^{\gamma''}$ is positive and nearly constant at all times in the evolution. This is because the relationship between pressure and density is set primarily by the equation of state of the gas, equation (18), whereas the relationship between temperature and density is controlled primarily by radiative equilibrium.

This simulation of thermal instability demonstrates how the relationships between pressure, temperature, and density can change dramatically at densities that are approximately the same as the critical densities for gravitational instability in cores of a few solar masses. The ability of the gas to change its effective equation of state may be important in facilitating the formation of gravitationally stable cores (Ballesteros-Paredes et al. 1999; Jappsen et al. 2005). The thermal instability improves the chances for the formation of gravitationally bound and yet stable cores, since the instability prevents gravitational collapse of some cores that would otherwise be unstable. For example, cores of 5 $M_{\odot}$ with initial central densities between 10^5 and 10^6 cm^{-3} are unstable to thermal expansion and do not collapse. Cores with 5 $M_{\odot}$ and lower densities are gravitationally stable, as expected. Cores with 5 $M_{\odot}$ and densities higher than 10^6 cm^{-3} always collapse.

7. CONCLUSIONS

A comparison of the observed and theoretically predicted properties of dark cloud cores suggests that the cores are gravitationally bound dynamical units with a density structure set by the approximate force balance between gravity and thermal pressure and a temperature structure set by radiative equilibrium with the general interstellar radiation field. Such gravitationally bound structures might exist in hydrodynamic equilibrium below the inertial range at the lower end of the supersonic turbulent cascade.

The interstellar turbulence should generate cores in a range of densities and masses, all below the sonic limit of the turbulent cascade, some that are gravitationally stable and some that are unstable. The stable cores are in general less dense, more

extended, and warmer. The unstable cores are denser, more centrally concentrated, and colder. Their velocities are generally inward, progressing toward free-fall collapse. Most of the observed cores can be classified into stable and unstable categories on the basis of these properties.

Our hydrodynamic study shows that cores may oscillate with periods of the sound crossing time, about one million years, if subjected to a modest external perturbation of pressure. Thus, stable starless cores could be long-lived in a modestly turbulent environment. While the one-dimensional model cores are permitted only radially symmetric oscillations, the dark cloud cores in a turbulent interstellar medium would be expected to have higher order oscillations. For example, the elliptical morphologies of many cores may be an expression of slow, asymmetric oscillations about a mean spherical equilibrium. Higher order oscillations have been inferred from observations of B68 (Alves et al. 2001).

There is no evolutionary path from the stable to the unstable cores; thus, not all observed cores are evolving toward gravitational collapse and star formation. Stable cores may persist indefinitely until perturbed by changing external conditions.

Spectral line observations of molecules with different degrees of volatility can be used to distinguish the differences in properties in the centers of the cores and their envelopes. The rate at which molecules freeze out of the gas phase onto dust grains is dependent on the collisions with dust grains and hence the density. More volatile species remain in the gas phase at higher densities. Spectral lines of these molecules are generated in, and provide information on, the denser centers of the cores. Less volatile species are severely depleted in the dense core centers, and the spectral lines of these species are generated in and provide information on the envelopes of the cores.

Because the gas temperature is determined predominantly by radiative equilibrium, the effective adiabatic index can change value and sign as the density and optical depth of the cores change with expansion or contraction. In particular, the rate of radiative cooling and hence the temperature of the gas are dependent on whether the gas density is above or below the critical density for effective collisional coupling of the gas and the dust. The reduction in the gas cooling rate at lower gas densities can create a thermal instability that causes the gas to heat up as it expands, further driving the expansion.

REFERENCES

Aikawa, Y., Ohashi, N., Inutsuka, S., Herbst, E., & Takakuwa, S. 2001, ApJ, 552, 639
Alves, J., Lada, C., & Lada, E. 2001, Nature, 409, 159
Bacmann, A., André, A. P., Puget, J.-L., Abergel, A., Bontemps, S., & Ward-Thompson, D. 2000, A&A, 361, 555
Ballesteros-Paredes, J., Klessen, R., & Vázquez-Semadeni, E. 2003, ApJ, 592, 188
Ballesteros-Paredes, J., Vázquez-Semadeni, E., & Scalo, J. 1999, ApJ, 515, 286
Beichman, C. A., Myers, P. C., Emerson, J. P., Harris, S., Mathieu, R., Benson, P. J., & Jennings, R. E. 1986, ApJ, 307, 337
Benson, P., & Myers, P. 1989, ApJS, 71, 89
Bergin, E. A., Alves, J., Huard, T., & Lada, C. J. 2002, ApJ, 570, L101
Bergin, E. A., Ciardi, D. R., Lada, C. J., Alves, J., & Lada, E. A. 2001, ApJ, 557, 209
Bergin, E. A., Langer, W. D., & Goldsmith, P. F. 1995, ApJ, 441, 222
Black, J. H. 1994, in ASP Conf. Ser. 58, First Symposium on the Infrared Cirrus and Diffuse Interstellar Clouds, ed. R. M. Cutri & W. B. Latter (San Francisco: ASP), 355
Bonnor, W. 1956, MNRAS, 116, 351
Brown, P., Charnley, S., & Millar, T. 1988, MNRAS, 231, 409
Burke, J., & Hollenbach, D. 1983, ApJ, 265, 223
Caselli, P., Benson, P. J., Myers, P. C., & Tafalla, M. 2002a, ApJ, 572, 238
Caselli, P., Walmsley, C. M., Tafalla, M., Dore, L., & Myers, P. C. 1999, ApJ, 523, L165
Caselli, P., Walmsley, C. M., Zucconi, A., Tafalla, M., Dore, L., & Myers, P. C. 2002b, ApJ, 565, 331
———. 2002c, ApJ, 565, 344
Chandrasekhar, S. 1939, An Introduction to the Study of Stellar Structure (Chicago: Univ. Chicago Press)
Colella, P., & Woodward, P. 1984, J. Comput. Phys., 54, 174
Crapsi, A., Caselli, P., Walmsley, C. M., Myers, P. C., Tafalla, M., Lee, C. W., & Bourke, T. L. 2005, ApJ, 619, 379
Crapsi, A., Caselli, P., Walmsley, C. M., Tafalla, M., Lee, C. W., Bourke, T. L., & Myers, P. C. 2004, A&A, 420, 957
Dame, T. M., Elmegreen, B. G., Cohen, R. S., & Thaddeus, P. 1986, ApJ, 305, 892
Elmegreen, B. 2000, ApJ, 530, 277
Elmegreen, B., & Scalo, J. 2004, ARA&A, 42, 211
Evans, N. J., II, Rawlings, J. M. C., Shirley, Y. L., & Mundy, L. G. 2001, ApJ, 557, 193
Falgarone, E., & Puget, J. L. 1985, A&A, 142, 157
Field, G. 1965, ApJ, 142, 531
Foster, P., & Chevalier, R. 1993, ApJ, 416, 303
Fuller, G., & Myers, P. 1992, ApJ, 384, 523
Goldsmith, P. 2001, ApJ, 557, 736
Gonçalves, J., Galli, D., & Walmsley, M. 2004, A&A, 415, 617
Goodman, A. A., Barranco, J. A., Wilner, D. J., & Heyer, M. H. 1998, ApJ, 504, 223
Gregersen, E. M., & Evans, N. J., II. 2000, ApJ, 538, 260
Gregersen, E. M., Evans, N. J., II, Zhou, S., & Choi, M. 1997, ApJ, 484, 256
Hasegawa, T., & Herbst, E. 1993, MNRAS, 261, 83
Hasegawa, T., Herbst, E., & Leung, C. 1992, ApJS, 82, 167
Hunter, C. 1977, ApJ, 218, 834
Jappsen, A.-K., Klessen, R. S., Larson, R. B., Li, Y., & Mac Low, M.-M. 2005, A&A, 435, 611
Keto, E., Rybicki, G. B., Bergin, E. A., & Plume, R. 2004, ApJ, 613, 355
Klessen, R. S., Ballesteros-Paredes, J., Vázquez-Semadeni, E., & Durán-Rojas, C. 2005, ApJ, 620, 786
Krügel, E., & Siebenmorgen, R. 1994, A&A, 288, 929
Lada, C. J., Bergin, E. A., Alves, J. F., & Huard, T. L. 2003, ApJ, 586, 286
Larson, R. 1973, Fundam. Cosmic Phys., 1, 1
———. 1981, MNRAS, 194, 809
———. 1985, MNRAS, 214, 379
Launhardt, R., Evans, N. J., II, Wang, Y., Clemens, D. P., Henning, T., & Yun, J. L. 1998, ApJS, 119, 59
Lee, C. W., & Myers, P. C. 1999, ApJS, 123, 233
Lee, C. W., Myers, P. C., & Plume, R. 2004a, ApJS, 153, 523
Lee, C. W., Myers, P. C., & Tafalla, M. 1999b, ApJ, 526, 788
———. 2001, ApJS, 136, 703
Lee, J.-E., Bergin, E. A., & Evans, N. J., II. 2004b, ApJ, 617, 360
Leung, C. M., Kutner, M. L., & Mead, K. N. 1982, ApJ, 262, 583
Mac Low, M.-M., & Klessen, R. S. 2004, Rev. Mod. Phys., 76, 125
McKee, C. F., & Zweibel, E. G. 1995, ApJ, 440, 686
McLaughlin, D., & Pudritz, R. 1997, ApJ, 476, 750
Myers, P. C. 1983, ApJ, 270, 105
Myers, P. C., & Benson, P. J. 1983, ApJ, 266, 309
Myers, P. C., Linke, R. A., & Benson, P. J. 1983, ApJ, 264, 517
Nakano, T. 1998, ApJ, 494, 587
Ossenkopf, V., & Henning, T. 1994, A&A, 291, 943
Padoan, P. 1995, MNRAS, 277, 377
Pagani, L., et al. 2003, A&A, 406, L59
———. 2004, A&A, 417, 605
Redman, M. P., et al. 2005, MNRAS, submitted
Richtmyer, R. D. 1957, Difference Methods for Initial-Value Problems (New York: Interscience)
Sanders, D. B., Scoville, N. Z., & Solomon, P. M. 1985, ApJ, 289, 373
Scalo, J., & Elmegreen, B. G. 2004, ARA&A, 42, 275
Shirley, Y. L., Evans, N. J., II, & Rawlings, J. M. C. 2002, ApJ, 575, 337
Shirley, Y. L., Evans, N. J., II, Rawlings, J. M. C., & Gregersen, E. M. 2000, ApJS, 131, 249
Shu, F. H. 1977, ApJ, 214, 488
Sohn, J., Lee, C. W., Lee, H. M., Park, Y.-S., Myers, P. C., Lee, Y., & Tafalla, M. 2004, J. Korean Astron. Soc., 37, 261
Stamatellos, D., & Whitworth, A. P. 2003, A&A, 407, 941
Tafalla, M., Mardones, D., Myers, P., Caselli, P., Bachiller, R., & Benson, P. 1998, ApJ, 504, 900
Tafalla, M., Myers, P. C., Caselli, P., & Walmsley, C. M. 2004, A&A, 416, 191
Vázquez-Semadeni, E., Ballesteros-Paredes, J., & Klessen, R. S. 2003, ApJ, 585, L131
Wang, Y., Evans, N. J., II, Zhou, S., & Clemens, D. P. 1995, ApJ, 454, 217

Ward-Thompson, D., Motte, F., & André, P. 1999, MNRAS, 305, 143
Ward-Thompson, D., Scott, P. F., Hills, R. E., & André, P. 1994, MNRAS, 268, 276
Ward-Thompson, D., André, P., & Kirk, J. M. 2002, MNRAS, 329, 257
Whitworth, A. P., & Ward-Thompson, D. 2001, ApJ, 547, 317
Willacy, K., & Williams, D. A. 1993, MNRAS, 260, 635
Williams, J. P., Myers, P. C., Wilner, D. J., & Di Francesco, J. 1999, ApJ, 513, L61
Young, C. H., Shirley, Y. L., Evans, N. J., II, & Rawlings, J. M. C. 2003, ApJS, 145, 111
Zhou, S., Evans, N. J., II, Wang, Y., Peng, R., & Lo, K. Y. 1994, ApJ, 433, 131
Zucconi, A., Walmsley, C. M., & Galli, D. 2001, A&A, 376, 650

Note added in proof.—Concerning the discrepancy to which we refer in the introduction between the velocities within observed and modeled cores in the study of Ballesteros-Paredes et al. (2003), a recent study by Klessen et al. (2005) addresses this by focusing on model cores produced by gravoturbulent fragmentation that have subsonic velocities.